Catalysis Today xxx (xxxx) xxx–xxx

Contents lists available at ScienceDirect

Catalysis Today

journal homepage: www.elsevier.com/locate/cattod

High performance and toxicity assessment of Ta_3N_5 nanotubes for photoelectrochemical water splitting

Kaiqi Xu[a], Athanasios Chatzitakis[a,*], Sanne Risbakk[c], Mingyi Yang[b,c], Paul Hoff Backe[b,c], Mathieu Grandcolas[e], Magnar Bjørås[b,d], Truls Norby[a,*]

[a] Centre for Materials Science and Nanotechnology, Department of Chemistry, University of Oslo, FERMiO, Gaustadalléen 21, NO-0349 Oslo, Norway
[b] Department of Microbiology, Oslo University Hospital HF, Oslo, Norway
[c] Department of Medical Biochemistry, Institute for Clinical Medicine, University of Oslo, Oslo, Norway
[d] Department of Clinical and Molecular Medicine, Faculty of Medicine and Health Sciences, Norwegian University of Science and Technology (NTNU), PO Box 8905, NO-7491 Trondheim, Norway
[e] SINTEF Industry, Department of Materials and Nanotechnology, Group of Nano and Hybrid Materials, Oslo, Norway

ARTICLE INFO

Keywords:
Tantalum nitride
Nanotubes
Photoelectrochemical water splitting
Hydrogen
Electrodeposition
Toxicity

ABSTRACT

In this work, Co-based cocatalysts are electrodeposited on mesoporous Ta_3N_5 nanotubes. The electrodeposition time is varied and the optimized photoelectrode reaches a photocurrent density of 6.3 mA/cm^2 at 1.23 V vs. SHE, under simulated solar illumination of 1 Sun, in 1 M NaOH. The best performing electrode, apart from the high photocurrent density, shows improved stability under intense photoelectrochemical water splitting conditions. The dual function of the cocatalyst to improve not only the photoelectrochemical performance, but also the stability, is highlighted. Moreover, we adopted a simple protocol to assess the toxicity of Co and Ta contained nanostructured materials (representing used photoelectrodes) employing the human cell line HeLa S3 as target cells.

1. Introduction

Photoelectrochemical (PEC) water splitting provides a direct way to store solar energy in the form of hydrogen [1–3]. Intensive research is underway to develop materials that can bring this technology to a commercial level. Although more than 40 years have passed since Honda and Fujishima demonstrated the concept of PEC water splitting [4], there is still a long way to go. A viable PEC water splitting device should contain photoelectrodes that can produce 8 mA/cm^2 at an externally applied potential of no more than 0.8 V and a 15-year lifetime expectancy [1]. In fact, unbiased water splitting will be the ideal solution, which can be achieved through photovoltaic-assisted PEC water splitting with buried PV junctions [5–9]. The remaining problems are related to the development of efficient semiconducting electrodes, i.e. photoabsorbers, as well as efficient cocatalysts based on earth-abundant elements [10,11].

Tantalum nitride, Ta_3N_5, is an n-type semiconductor, which has been extensively studied by the PEC community because of its suitable bandgap energy (2.1 eV), as well as band positioning for overall water splitting [12–15]. In addition, Ta_3N_5 can theoretically reach photocurrent densities of approx. 13 mA/cm^2, more than enough for commercial exploitation [16]. Unfortunately, Ta_3N_5 is not stable and photocorrodes during short PEC operating times (20 − 30 min) as the anode photoelectrode [16,17]. One strategy to improve in general the stability of such photoelectrodes is through nanostructuring [18]. In this case, the photocurrent density is spread over a much larger area compared to a film electrode. Another strategy is to passivate the semiconductor surface by coating it with an electronically “leaky” oxide, such as TiO_2 [19,20] or with a cocatalyst [21]. The latter is particularly interesting as the appropriate cocatalyst can improve the sluggish surface electrochemical kinetics of the semiconductor and at the same time protect the buried photoabsorbing surface. Moreover, the direct junction between the semiconductor and the cocatalyst is preferred over a configuration where an ALD-formed or another passive layer (e.g. ferrihydrite) is interfered between the photoabsorber and the cocatalyst, where a reduction in the photocurrent density is observed [22].

Earlier works have reached impressive photocurrent densities and in some cases stable performances over a few hours of PEC operation. Liu et al. [22] have reached 8.5 mA/cm^2 in alkaline conditions for Co_3O_4 coated Ta_3N_5 films, which were grown by a combination of anodization and hydrothermal methods on Ta substrate. The cocatalyst was loaded

* Corresponding authors.
E-mail addresses: a.e.chatzitakis@smn.uio.no (A. Chatzitakis), truls.norby@kjemi.uio.no (T. Norby).

https://doi.org/10.1016/j.cattod.2019.12.031
Received 1 October 2019; Received in revised form 12 December 2019; Accepted 26 December 2019

by a hydrothermal method. The stability of this electrode was however very poor, and after 2 h, 70 % of the activity was lost. The authors improved dramatically the stability by adding a protective layer of ferrihydrite, which was chemical grown on the porous cubic Ta_3N_5 films. Although the stability was improved, the photocurrent density at 1.23 V vs. SHE was reduced to 5.2 mA/cm^2. Wang et al. [23] coated Ta_3N_5 nanotubes with a combination of NiFe LDH and Co-Pi/Co(OH)$_x$ as the cocatalyst and they achieved 6.3 mA/cm^2 at 1.23 V vs. SHE and a stability retention of approx. 90 % after 2 h of operation. In a subsequent work, the same group reported the same photocurrent density without the use of NiFe LDH. Unfortunately, the stability was not assessed, although the authors highlighted that this was the highest performance ever achieved for such a nanostructured electrode [24]. The improved photocurrent density without the NiFe LDH is attributed to the formation of a subnitride layer between the nanotubes and the Ta substrate. An earlier work by Khan et al. [25] reported a photocurrent density of 7.4 mA/cm^2 at 1.23 V vs. SHE without the use of cocatalysts. The stability was not assessed, but the low faradaic efficiency of the hydrogen evolution in the cathode suggests a poor stability of the material. Nevertheless, the authors highlighted the ability of bare Ta_3N_5 nanotubes to reach such high photocurrent densities by only tuning the microstructural properties. To conclude with this short literature review on the performance and stability of Ta_3N_5 nanotubes we refer to the work of He et al. [17]. The authors elucidated that the self-oxidation of Ta_3N_5 and the formation of a thin (approx. 3 nm) oxide film are responsible for the complete suppression of the activity of the material. The complete isolation of Ta_3N_5 from water or any other oxidizing species is necessary. For this reason, a protective layer of ALD-coated MgO was applied together with a surface modification with Co(OH)$_x$ as the cocatalyst. The cocatalyst was loaded by simply dipping the electrode in a solution of Co^{2+} ions. At 1.23 V vs. SHE the optimized photoelectrode reached approx. 7 mA cm^{-2}, but the stability was assessed for only 30 min and during this period approx. 10 % decrease in the performance is witnessed.

It should be mentioned that in all the cases above, the deposition of the Co-based cocatalysts is mainly done by chemical methods, which are not really controlled or optimized. In this work, we are continuing on our previous efforts to improve both the photocurrent density, as well as the stability of Ta_3N_5 nanotubes [21]. We have already demonstrated a photocurrent density of 2.3 mA/cm^2 at 1.23 V vs. SHE on Co(OH)$_x$/Co-Pi coated Ta_3N_5 nanotubes and an improvement in the stability of more than 20 % compared to the bare Ta_3N_5 nanotubes [21]. The main aim presently is the optimization of the electrodeposition of the cocatalyst and as we will see, it plays a significant role in the performance of Ta_3N_5 nanotubes. The long-term stability still remains an issue though, but an optimized cocatalyst deposition can significantly improve it. Therefore, fine-tuning of the cocatalyst coverage is important in order to improve the stability without interfering additional protective layers. Additionally, and in an effort to assess the environmental impact of such nanomaterials, we performed a toxicity evaluation of used Ta_3N_5 nanotubes with and without Co-based cocatalysts. Such an approach is uncommon, but extremely important and we hope to raise awareness for responsible research and innovation, as well as to showcase a simple method to monitor the potential environmental impact of such nanomaterials.

2. Experimental

2.1. Materials

Ta foil (0.25 mm thick, 99.9 % purity) was purchased from GoodFellow and used as the substrate during anodization. All the other chemicals were of analytical grade from Sigma-Aldrich and used without further treatment. Deionized water (18.2 MΩ cm) was used for the preparation of all the solutions. NH_3 (standard cooling quality, ≥ 99.92 %) and N_2 5.0 were both obtained from Nippon Gases.

2.2. Preparation of Ta_3N_5 nanotubes

The growth of Ta_3N_5 nanotubes is based on our previous work [21] with some modifications. For instance, after the initial cleaning procedure of the Ta foil, the first Ta_2O_5 nanotubes layer was grown under 60 V for 5 min, then rinsed with DI water and removed by an intense airflow from an air compressor. The new Ta_2O_5 nanotubes layer grown under 60 V for 30 min was then stabilized in ethanol for 5 min, before being transferred to a ProboStat™ for nitridation. The conversion of Ta_2O_5 nanotubes to Ta_3N_5 nanotubes was performed by annealing the oxide in a flow of NH_3 (15 sccm) at 950 °C for 2 h, then cooled down under the same NH_3 stream with a rate of 5 °C /min.

2.3. Electrodeposition of Co-based cocatalysts

We chose to electrodeposit the Co-based cocatalysts directly on our Ta_3N_5 nanotubes, rather than the simple physical implementation reported in the literature [24,26,27]. The purpose is to have a better control of the deposition quality and conditions by an optimization of the deposition parameters, and to provide good repeatability for scaling up purposes.

The Co(OH)$_X$ cocatalyst was electrodeposited according to the Pourbaix diagram of the Co species [28] in a three-electrode electrochemical cell with Ta_3N_5 nanotubes, standard calomel electrode (SCE) and Pt foil as the working, reference and counter electrodes, respectively. A potential of -0.5 V vs. SCE was applied on the working electrode for 15 ~ 480 s in a stirred solution containing 0.05 M $Co(NO_3)_2$, at pH 11 ± 0.5, which was constantly monitored by a pH meter (HORIBA D-71 G, Japan).

Cobalt-phosphate (Co-Pi) cocatalyst was also electrodeposited with modification based on the pioneering work of Nocera et al. [29]. For instance, a potential of 0.85 V vs. SCE was applied on the Co(OH)$_X$ loaded working electrode for 15 ~ 480 s, in a solution containing 0.05 mM $Co(NO_3)_2$ in 0.1 M potassium phosphate buffer (pH 7). In this way a potential controlled electrolysis of Co^{2+} salts in phosphate (Pi) buffer solution is occurring and as a result Co-Pi is formed with a predominant biscubane structure of Co_3PO_4-Co [30,31]. Afterwards, the electrode was rinsed with DI water and dried in ambient air.

2.4. Characterization and PEC measurements

The microscopic images were obtained with a Hitachi SU8230 ultra-high resolution cold-field emission SEM equipped with a secondary electron (SE) detector under an acceleration voltage of 10 kV. The Ta_3N_5 phase was confirmed using a Rigaku MiniFlex 600 XRD with a Cu (α) 1 radiation source (λ = 1.5046 Å), step 0.01° (2θ) and a scan rate of 1° min^{-1}.

The same three-electrode configuration was used for PEC performance of the different photoelectrodes, in a 1 M NaOH (pH 13.6) electrolyte, which was purged with N_2 prior to all experiments. All the electrochemical/photoelectrochemical measurements were conducted by a Gamry Reference 3000 potentiostat, under 1 sun simulated solar light from a Newport Oriel® LCS-100 solar simulator equipped with a 100 W ozone-free xenon lamp and an AM 1.5 G filter. The light intensity was regularly calibrated by a monocrystalline Si PV reference cell (Newport 91150V-KG5). The hydrogen evolution experiments were conducted in a two-electrode configuration where a Pt sheet was used as the cathode electrode. Hydrogen production was measured and quantified by an Agilent micro GC 3000 equipped with a molecular sieve column. Potentials were corrected vs. SHE according to the Nernst equation:

$$E_{SHE} = E_{meas.} + 0.059 \times pH + 0.241\,V.$$

2.5. Materials toxicity test

2.5.1. Photoelectrode extractions

The used photoelectrodes were washed in 70 % ethanol once, and twice in DI water. Afterwards, they were packed in aluminum foil and autoclaved at 134 °C for 30 min. Based on the ISO standard (ISO 10993-12) guide, the photoelectrodes (about 1.5 cm^2, thickness 0.5-1 mm, final 3 cm^2/ml) were soaked in 0.5 ml Dulbecco's modified Eagle's medium (DMEM) in a 50 ml vial at 37 °C for 24 h.

2.5.2. Cell culture

Human cell line HeLa S3 was purchased from American Type Culture Collection (ATCC). The cells were normally cultured at 37 °C with 5 % CO_2 in DMEM including 4.5 % glucose (Biowhittaker, Cambrex Inc.) and supplemented with 10 % fetal calf serum, 100 IU/ml penicillin and 100 µg/ml streptomycin.

2.5.3. 3-(4,5-dimethylthiazol-2-yl)-2,5-diphenyltetrazolium (MTT) assay

The cells were seeded at 20 % confluence in a 96-well plate and cultured overnight to allow cell adhesion. Then the cells were exposed to photoelectrode extracts for the indicated 48 h in DMEM. The cell viability was determined by the MTT assay using the Cell Proliferation kit (Roche Diagnostics). The assay is based on the cleavage of the yellow tetrazolium salt MTT to purple formazan crystals by metabolic active cells. The formazan was quantified by measuring the absorbance at 570 nm and a reference wavelength at 690 nm on a microplate reader (Epoch, by BioTek Instrument Inc.). Each sample was measured in triplicate wells. The cell viability was calculated as percentage relative to control cells.

3. Results and discussion

Fig. 1(a) shows a typical cross-section SEM image of Ta_3N_5 nanotubes grown firstly through anodization, followed by nitridation under high temperature ammonolysis. The length of the nanotubes is more than 30 µm, providing a high surface area photoelectrode. The mesoporous structure shown in Fig. 1(b) may further increase the surface area of the photoelectrode. After electrodeposition of the cocatalysts, the smooth outer walls of the nanotubes are covered by nanoparticles, which are marked in dashed circles, indicating the successful loading of the cocatalysts (Fig. 1(c)). The XRD pattern in Fig. 1(d) matches that of the standard Ta_3N_5 (COD® ID1005006), indicating that after 2 h treatment in NH_3, the Ta_2O_5 nanotubes were successfully converted into Ta_3N_5. The XRD pattern shows no other phases, highlighting the increased crystallinity and phase purity of the Ta_3N_5 nanotubes.

As stated earlier, the main objective of this work was to examine and optimize the correlation between the PEC performance and the electrodeposition time of the cocatalysts. According to our previous work [21], without $Co(OH)_x$, the photocurrent of bare Ta_3N_5 nanotubes is typically under 1 mA/cm^2 @ 1.23 V vs. SHE, much smaller than the theoretical limit for Ta_3N_5 of 13 mA/cm^2. One reason is that pure Ta_3N_5 suffers from poor charge transfer kinetics from the surface to the electrolyte [16]. Thus, the electrodeposition of $Co(OH)_x$, even as short as 15 s, can significantly increase the photocurrent to 3.5 mA/cm^2 @ 1.23 V vs. SHE, as seen in Fig. 2(a). From the same figure and for the different electrodeposition times for $Co(OH)_x$, the best PEC performance is given by the sample deposited for 30 s, showing a photocurrent density as high as 4.8 mA/cm^2 @ 1.23 V vs. SHE. A prolonged deposition time does not enhance the performance further, and a decreasing trend is witnessed when the deposition time is increased from 30 s to 480 s. Diffuse reflectance spectroscopy (DRS) measurements show the typical optical absorption spectra of Ta_3N_5, with an onset at approx. 610 nm, which corresponds to 2.03 eV (Fig. S1 in the Supplementary Information). The presence of $Co(OH)_X$ and Co-Pi slightly enhances the light absorption at shorter wavelengths compared to the absorption onset, indicating that the Co-based cocatalysts not only facilitate the interfacial charge transfer kinetics, but also the utilization of more visible light. A 20 min chronoamperometric test on those samples at 1.1 V vs. SHE is shown in Fig. 2(b), where the photocurrent densities are consistent with the ones obtained in the j-U curves of Fig. 2(a).

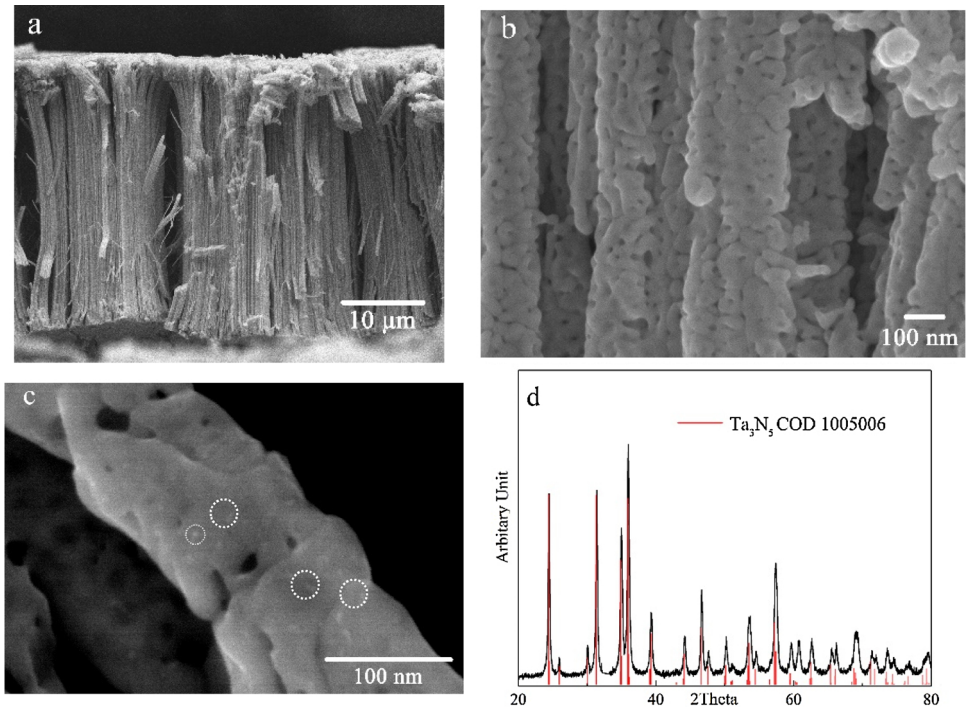

Fig. 1. SEM images of Ta_3N_5 nanotubes after anodization and ammonolysis: (a) cross-sectional view, (b) mesoporous structure of the nanotube walls under increased magnification, (c) cocatalyst nanoparticles (marked with dashed circles) present on the outer wall of a single nanotube after electrodeposition (image corresponds to the TaN/$Co(OH)_x$/Co-Pi 30 s 60 s sample), and (d) XRD of freshly made Ta_3N_5 nanotubes, fitted according to the COD® crystallographic database with ID 1005006.

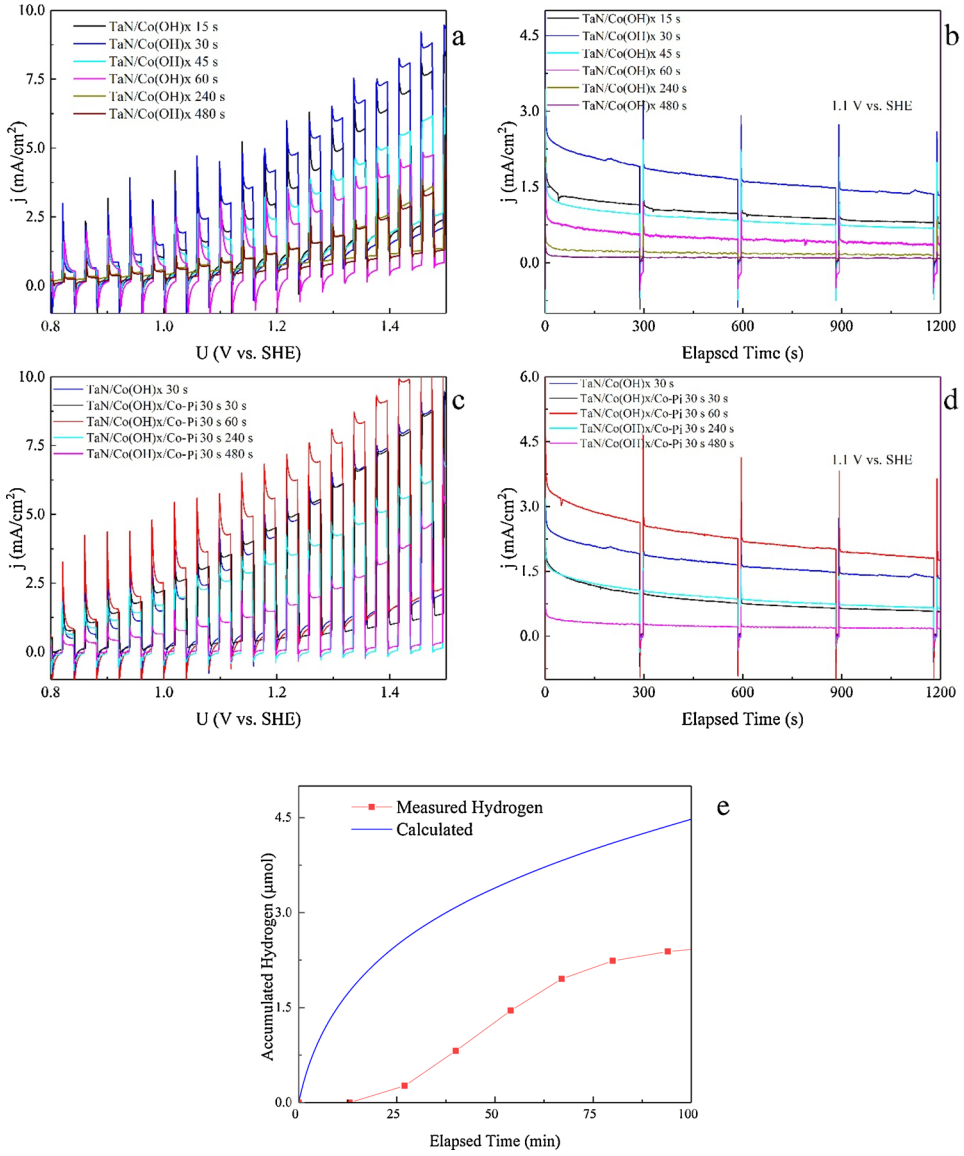

Fig. 2. j-U plots of Ta_3N_5 nanotubes electrodeposited with $Co(OH)_X$ under different deposition time; (b) stability tests of the samples mentioned in Fig. 2 (a), under 1 sun @ 1.1 V vs. SHE for 20 min; (c) j-U plots of Ta_3N_5 nanotubes firstly loaded with $Co(OH)_x$ for 30 s, and subsequently electrodeposited with Co-Pi under varying deposition times; (d) stability tests of the samples mentioned in Fig. 2 (c), under the same conditions; (e) hydrogen evolution at 1.23 V vs. SHE in a two-electrode system with TaN/Co(OH)x/Co-Pi 30 s 60 s as anode and Pt as the cathode.

A further modification by co-deposition of Co-Pi has been proven to further enhance the performance and stability of the Ta_3N_5 nanotubes. Fig. 2(c) shows that a 30 s deposition of Co-Pi after 30 s deposition of Co $(OH)_x$ does not provide any noticeable increase in the PEC performance. A 60 s deposition of Co-Pi though can significantly increase the photocurrent density, reaching 6.3 mA/cm^2 @ 1.23 V vs. SHE, providing a more than 30 % increase in the PEC performance compared to the optimized sample loaded with only $Co(OH)_x$. A similar decreasing trend in the PEC performance can also be witnessed as the Co-Pi deposition time increases from 30 s to 480 s. A synergy effect of the combination of the two cocatalysts at the optimized composition is explained in the SI (see Fig. S2 and corresponding analysis). The stability test in Fig. 2(d) shows a close to 50 % degradation of the performance for the optimized sample, though its photocurrent remains the highest after 20 min at 1.1 V vs. SHE. The degradation can also be witnessed in Fig. 2(e), where the H_2 concentration (red curve) significantly deviates from the theoretically expected one (blue curve). Assuming a 100 % efficiency of the Pt cathode, it is evident that part of the photocurrent is participating in the corrosion of the photoelectrode.

Table 1
Stability loss after a 20 min PEC test at 1.1 V vs. SHE under 1 sun simulated illumination, and charge transfer resistance in the photoelectrode/liquid interface as obtained by EIS at 1.23 V vs. SHE under 1 sun simulated illumination.

Photoelectrode	Stability loss (%)	R_{ct} (Ω cm^2)
Co(OH)x series		
TaN/$Co(OH)_x$ 15s	55	458
TaN/$Co(OH)_x$ 30 s	**51**	**294**
TaN/$Co(OH)_x$ 45s	55	327
TaN/$Co(OH)_x$ 60s	62	1096
TaN/$Co(OH)_x$ 240s	65	1422
TaN/$Co(OH)_x$ 480s	64	2059
Co(OH)x/Co-Pi series		
TaN/$Co(OH)_x$/Co-Pi 30 s 30 s	70	925
TaN/$Co(OH)_x$/Co-Pi 30 s 60 s	**52**	**199**
TaN/$Co(OH)_x$/Co-Pi 30 s 240 s	62	830
TaN/$Co(OH)_x$/Co-Pi 30 s 480 s	70	994

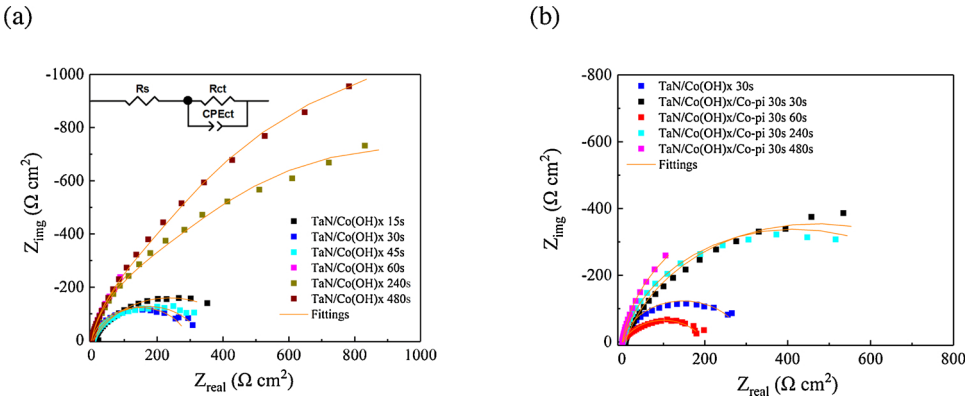

Fig. 3. Nyquist plots of the different photoelectrodes recorded at 1.23 V vs. SHE under 1 sun simulated illumination. The frequency range was 100 kHz to 100 mHz, while the amplitude of the sinusoidal voltage was 10 mV rms. All fittings are shown by the orange lines. The equivalent circuit used to fit the raw data is depicted in (a).

In general, all the photoelectrodes lose a significant fraction of their photocurrent density. As it can be seen from Table 1 the stability loss varies between 50 and 70 % after 20 min of PEC operation at 1.1 V vs. SHE under 1 sun simulated illumination. It should be highlighted though that the optimized photoelectrodes showed the lowest photocurrent loss under the measured conditions, 51 and 52 % for the Co $(OH)_x$ and $Co(OH)_x$/Co-Pi, respectively. It should be added that they were operating at significantly higher photocurrent densities, therefore their photocorrosion rate was smaller than the rest of the samples. Moreover and taking into account the surface morphology of the co-catalyst loaded nanotubes (Fig. 1(c)), a homogeneous cocatalyst film will certainly improve further the stability of Ta_3N_5, in addition to the OER kinetics. Nevertheless, the Co mass loading of the TaN/$Co(OH)_x$/Co-Pi 30 s 60 s sample from the chronoamperometric curves equals to 6.5 10^{-4} g/cm^2 (see SI).

Electrochemical impedance spectroscopy (EIS) was used in order to further confirm the improved overall charge transfer kinetics of the optimized photoelectrodes. Fig. 3 shows the Nyquist plots obtained at 1.23 V vs. SHE under 1 sun illumination. The magnitude of the semicircles in the Nyquist curves is a measure of the magnitude of the resistance during PEC operation. The smaller the semicircle, the lower the overall charge transfer resistance. It can be seen that the 30 s $Co(OH)_x$ and 30 s 60 s $Co(OH)_x$/Co-Pi modified Ta_3N_5 nanotubes have the lowest overall charge transfer resistance in the photoelectrode/electrolyte interface. The EIS plots were deconvoluted using a simple Randles circuit and the total resistance for each sample is given in Table 1. It should be noted that EIS is not a fingerprint method and several equivalent electrical circuits can be fitted to certain raw data values. In the present case, we were interested in the total charge transfer resistance, which includes the film and interfacial resistances, and for this reason a Randles circuit (inset in Fig. 3a) was employed and gave reasonable fittings. It can be seen that the total resistance is reduced by 30 % when Co-Pi is co-deposited on the $Co(OH)_x$ loaded Ta_3N_5 nanotubes. More information and the rest of the fitted parameters can be found in the SI.

As stated in the introductory part, some of the used photoelectrodes were subjected to a toxicity assessment. To evaluate the toxicity of the photoelectrodes, we performed the MTT assay to determine the affection of the photoelectrode extracts on human cell proliferation in vitro. We selected a few random samples, including the best performing photoelectrode, as assessed earlier. The toxicity tests were carried out in triplicate using 1/1 dilutions. In the cell culture, we used the human cell line Hela as the target cells, which were derived from cervical cancer cells and are commonly used in vitro viability assays. The cells viability is shown in Fig. 4. In comparison to the negative control, only the TaN/$Co(OH)_x$/Co-Pi 30 s 60 s showed a slight reduction in the cell viability with a significant standard deviation. We also used hydrogen peroxide (H_2O_2) as the positive control, as H_2O_2 is known to possess a high cytotoxicity, which results in protein, lipid and DNA oxidation. As

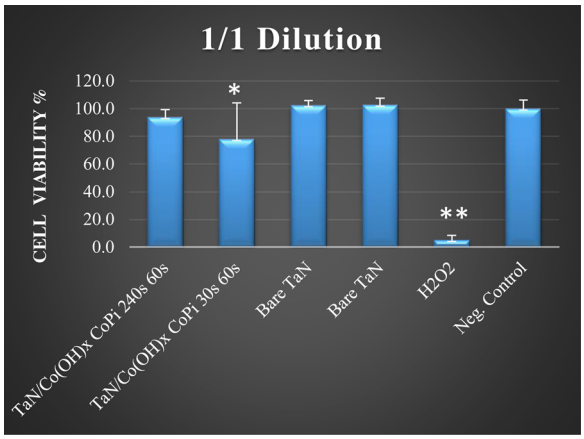

Fig. 4. Cytotoxicity of used photoelectrodes after 48 h exposure in cell cultures. The photoelectrode extract solutions were diluted with culture medium at a concentration of 1/1 and incubated with HeLa cells in 96 wells. The cell viability was measured by optical absorbance at 590 nm with the MTT assay. H_2O_2 was used as positive control with concentration of 1 mM for 1/1 dilution. The negative control was mocked with cell culture medium. n = 9 from triplicates experiments. Error bars represent mean + SD. p value from two-tails Student's *T* test. *p < 0.05. ** p < 0.01.

expected, the 1/1 dilution (final concentration at 1 mM) caused a significant decrease in the cell viability. Importantly, the bare Ta_3N_5 nanotubes showed no cytotoxicity on the human cell line Hela. Therefore, we speculate that the observed toxicity of the cocatalyst modified samples is due to the Co element [32–34].

4. Conclusions

In conclusion, we have surface modified highly crystalline Ta_3N_5 nanotubes with a cocatalyst based on $Co(OH)_x$ and Co-Pi, which were electrodeposited from solutions of their salts in order to increase the sluggish interfacial kinetics for water oxidation. The electrodeposition time was varied between 15 s and 480 s and the optimized photoelectrode was synthesized after deposition of $Co(OH)_x$ for 30 s and 60 s for Co-Pi. The optimized photoelectrode reached a photocurrent density of 6.3 mA/cm^2 at 1.23 V vs. SHE under 1 sun simulated illumination in 1 M NaOH. This photocurrent density is among the highest reported in the literature. Moreover, the best performing photoelectrodes apart from their high current densities, showed improved stability under intense PEC operating conditions. Electrodeposition is a facile method, which allows good control over sample modification with a cocatalyst and flexibility in the synthesis conditions. Fine-tuning of the electrodeposition parameters and quality of the cocatalyst coating may be of

dual importance, which is to improve the interfacial kinetics, as well as to protect the underlying photoelectrode.

Finally, in an effort to conduct responsible research and innovation, we assessed the toxicity of some used photoelectrodes by the MTT assay. The human cell line Hela S3 was used as the target cell and our results indicate that the Ta_3N_5 nanotubes do not show any toxicity. Co-modified Ta_3N_5 nanotubes showed a slight decrease in the cell viability, which should be taken into account when Co containing compounds are involved. Future works should also address the toxicity of the electrolysis solutions, which may be contaminated by Co leaching.

CRediT authorship contribution statement

Kaiqi Xu: Conceptualization, Methodology, Validation, Investigation, Writing - original draft, Writing - review & editing, Visualization. **Athanasios Chatzitakis:** Conceptualization, Methodology, Validation, Writing - original draft, Writing - review & editing, Visualization, Supervision, Project administration, Funding acquisition. **Sanne Risbakk:** Investigation. **Mingyi Yang:** Conceptualization, Methodology, Investigation, Validation, Writing - original draft, Supervision, Funding acquisition. **Paul Hoff Backe:** Conceptualization, Methodology, Investigation, Validation, Writing - original draft, Supervision, Funding acquisition. **Mathieu Grandcolas:** Investigation. **Magnar Bjørås:** Conceptualization, Methodology, Supervision, Funding acquisition. **Truls Norby:** Conceptualization, Methodology, Writing - original draft, Writing - review & editing, Supervision, Project administration, Funding acquisition.

Declaration of Competing Interest

The authors declare that there are no conflicts of interest.

Acknowledgement

Financial support from the Research Council of Norway (CO2BioPEC project 250261) is acknowledged.

Appendix A. Supplementary data

Supplementary material related to this article can be found, in the online version, at doi:https://doi.org/10.1016/j.cattod.2019.12.031.

References

[1] Roel van de Krol, M. Grätzel, Photoelectrochemical Hydrogen Production, Springer US2012.
[2] M. Grätzel, Photoelectrochemical cells, Nature 414 (2001) 338–344.
[3] R.J. Detz, J.N.H. Reek, B.C.C. van der Zwaan, The future of solar fuels: when could they become competitive? Energy Environ. Sci. 11 (2018) 1653–1669.
[4] A. Fujishima, K. Honda, Electrochemical photolysis of water at a semiconductor electrode, Nature 238 (1972) 37–38.
[5] S.Y. Reece, J.A. Hamel, K. Sung, T.D. Jarvi, A.J. Esswein, J.J.H. Pijpers, D.G. Nocera, Wireless solar water splitting using silicon-based semiconductors and earth-abundant catalysts, Science 334 (2011) 645.
[6] Y. Yamada, N. Matsuki, T. Ohmori, H. Mametsuka, M. Kondo, A. Matsuda, E. Suzuki, One chip photovoltaic water electrolysis device, Int. J. Hydrogen Energy 28 (2003) 1167–1169.
[7] S. Licht, B. Wang, S. Mukerji, T. Soga, M. Umeno, H. Tributsch, Efficient solar water splitting, exemplified by RuO2-catalyzed AlGaAs/Si photoelectrolysis, J. Phys. Chem. B 104 (2000) 8920–8924.
[8] O. Khaselev, J.A. Turner, A monolithic photovoltaic-photoelectrochemical device for hydrogen production via water splitting, Science 280 (1998) 425.
[9] F.F. Abdi, L. Han, A.H.M. Smets, M. Zeman, B. Dam, R. van de Krol, Efficient solar water splitting by enhanced charge separation in a bismuth vanadate-silicon tandem photoelectrode, Nat. Commun. 4 (2013) 2195.
[10] X. Sun, K. Xu, C. Fleischer, X. Liu, M. Grandcolas, R. Strandbakke, S.T. Bjørheim, T. Norby, A. Chatzitakis, Earth-abundant electrocatalysts in proton exchange membrane electrolyzers, Catalysts 8 (2018).
[11] A. Chatzitakis, E. Nikolakaki, S. Sotiropoulos, I. Poulios, Hydrogen production using an algae photoelectrochemical cell, Appl. Catal. B: Environ. 142-143 (2013) 161–168.
[12] W.-J. Chun, A. Ishikawa, H. Fujisawa, T. Takata, J.N. Kondo, M. Hara, M. Kawai, Y. Matsumoto, K. Domen, Conduction and valence band positions of Ta2O5, TaON, and Ta3N5 by UPS and electrochemical methods, J. Phys. Chem. B 107 (2003) 1798–1803.
[13] C. Zhen, R. Chen, L. Wang, G. Liu, H.-M. Cheng, Tantalum (oxy)nitride based photoanodes for solar-driven water oxidation, J. Mater. Chem. A 4 (2016) 2783–2800.
[14] P. Zhang, J. Zhang, J. Gong, Tantalum-based semiconductors for solar water splitting, Chem. Soc. Rev. 43 (2014) 4395–4422.
[15] E. Nurlaela, A. Ziani, K. Takanabe, Tantalum nitride for photocatalytic water splitting: concept and applications, Mater. Renew. Sustain. Energy 5 (2016) 18.
[16] G. Liu, S. Ye, P. Yan, F. Xiong, P. Fu, Z. Wang, Z. Chen, J. Shi, C. Li, Enabling an integrated tantalum nitride photoanode to approach the theoretical photocurrent limit for solar water splitting, Energy Environ. Sci. 9 (2016) 1327–1334.
[17] Y. He, James E. Thorne, Cheng H. Wu, P. Ma, C. Du, Q. Dong, J. Guo, D. Wang, What limits the performance of Ta3N5 for solar water splitting? Chemistry 1 (2016) 640–655.
[18] N.S. Lewis, Developing a scalable artificial photosynthesis technology through nanomaterials by design, Nat. Nanotechnol. 11 (2016) 1010.
[19] A. Paracchino, V. Laporte, K. Sivula, M. Grätzel, E. Thimsen, Highly active oxide photocathode for photoelectrochemical water reduction, Nat. Mater. 10 (2011) 456.
[20] M.F. Lichterman, K. Sun, S. Hu, X. Zhou, M.T. McDowell, M.R. Shaner, M.H. Richter, E.J. Crumlin, A.I. Carim, F.H. Saadi, B.S. Brunschwig, N.S. Lewis, Protection of inorganic semiconductors for sustained, efficient photoelectrochemical water oxidation, Catal. Today 262 (2016) 11–23.
[21] K. Xu, A. Chatzitakis, I.J.T. Jensen, M. Grandcolas, T. Norby, $Ta_3N_5/Co(OH)_X$ composites as photocatalysts for photoelectrochemical water splitting, Photochem. Photobiol. Sci. 18 (2019) 837–844.
[22] G. Liu, J. Shi, F. Zhang, Z. Chen, J. Han, C. Ding, S. Chen, Z. Wang, H. Han, C. Li, A Tantalum Nitride Photoanode Modified with a Hole-Storage Layer for Highly Stable Solar Water Splitting, Angew. Chemie Int. Ed. 53 (2014) 7295–7299.
[23] L. Wang, F. Dionigi, N.T. Nguyen, R. Kirchgeorg, M. Gliech, S. Grigorescu, P. Strasser, P. Schmuki, Tantalum nitride nanorod arrays: introducing Ni–Fe layered double hydroxides as a cocatalyst strongly stabilizing photoanodes in water splitting, Chem. Mater. 27 (2015) 2360–2366.
[24] L. Wang, X. Zhou, N.T. Nguyen, I. Hwang, P. Schmuki, Strongly enhanced water splitting performance of Ta_3N_5 nanotube photoanodes with subnitrides, Adv. Mater. 28 (2016) 2432–2438.
[25] S. Khan, M.J.M. Zapata, D.L. Baptista, R.V. Gonçalves, J.A. Fernandes, J. Dupont, M.J.L. Santos, S.R. Teixeira, Effect of oxygen content on the photoelectrochemical activity of crystallographically preferred oriented porous Ta3N5 nanotubes, J. Phys. Chem. C 119 (2015) 19906–19914.
[26] L. Wang, N.T. Nguyen, X. Zhou, I. Hwang, M.S. Killian, P. Schmuki, Enhanced charge transport in tantalum nitride nanotube photoanodes for solar water splitting, ChemSusChem 8 (2015) 2615–2620.
[27] Z. Su, S. Grigorescu, L. Wang, K. Lee, P. Schmuki, Fast fabrication of Ta_2O_5 nanotube arrays and their conversion to Ta_3N_5 for efficient solar driven water splitting, Electrochem. commun. 50 (2015) 15–19.
[28] E.M. Garcia, J.S. Santos, E.C. Pereira, M.B.J.G. Freitas, Electrodeposition of cobalt from spent Li-ion battery cathodes by the electrochemistry quartz crystal microbalance technique, J. Power Sources 185 (2008) 549–553.
[29] Y. Surendranath, M. Dincă, D.G. Nocera, Electrolyte-dependent Electrosynthesis and activity of cobalt-based water oxidation catalysts, J. Am. Chem. Soc. 131 (2009) 2615–2620.
[30] M.W. Kanan, Y. Surendranath, D.G. Nocera, Cobalt–phosphate oxygen-evolving compound, Chem. Soc. Rev. 38 (2009) 109–114.
[31] J.J. Pijpers, M.T. Winkler, Y. Surendranath, T. Buonassisi, D.G. Nocera, Light-induced water oxidation at silicon electrodes functionalized with a cobalt oxygen-evolving catalyst, Proc. Natl. Acad. Sci. 108 (2011) 10056–10061.
[32] S. Chattopadhyay, S.K. Dash, S. Tripathy, B. Das, D. Mandal, P. Pramanik, S. Roy, Toxicity of cobalt oxide nanoparticles to normal cells; an in vitro and in vivo study, Chem. Biol. Interact. 226 (2015) 58–71.
[33] A.A. Jensen, F. Tuchsen, Cobalt exposure and cancer risk, Crit. Rev. Toxicol. 20 (1990) 427–439.
[34] D.G. Barceloux, D. Barceloux, Cobalt, J. Toxicol. Clin. Toxicol. 37 (1999) 201–216.